2015-09

Measurement of transmission loss using an inexpensive mobile source on the Upper Slope of the South China Sea

Graessle, Samuel W.

Monterey, California: Naval Postgraduate School

NAVAL POSTGRADUATE SCHOOL

MONTEREY, CALIFORNIA

THESIS

MEASUREMENT OF TRANSMISSION LOSS USING AN INEXPENSIVE MOBILE SOURCE ON THE UPPER SLOPE OF THE SOUTH CHINA SEA

by

Samuel W. Graessle

September 2015

Thesis Advisor: Ching-Sang Chiu
Co-Advisor: Chris Miller

Approved for public release; distribution is unlimited

THIS PAGE INTENTIONALLY LEFT BLANK

REPORT DOCUMENTATION PAGE

Form Approved OMB No. 0704–0188

1. AGENCY USE ONLY *(Leave blank)*	**2. REPORT DATE** September 2015	**3. REPORT TYPE AND DATES COVERED** Master's Thesis

4. TITLE AND SUBTITLE
MEASUREMENT OF TRANSMISSION LOSS USING AN INEXPENSIVE MOBILE SOURCE ON THE UPPER SLOPE OF THE SOUTH CHINA SEA

5. FUNDING NUMBERS

6. AUTHOR(S) Graessle, Samuel W.

7. PERFORMING ORGANIZATION NAME(S) AND ADDRESS(ES)
Naval Postgraduate School
Monterey, CA 93943-5000

8. PERFORMING ORGANIZATION REPORT NUMBER

9. SPONSORING /MONITORING AGENCY NAME(S) AND ADDRESS(ES)
N/A

10. SPONSORING/MONITORING AGENCY REPORT NUMBER

11. SUPPLEMENTARY NOTES The views expressed in this thesis are those of the author and do not reflect the official policy or position of the Department of Defense or the U.S. Government. IRB Protocol number ____N/A____.

12a. DISTRIBUTION / AVAILABILITY STATEMENT
Approved for public release; distribution is unlimited

12b. DISTRIBUTION CODE

13. ABSTRACT (maximum 200 words)

During the 2014 South China Sea Upper-Slope Sand Dunes Experiment, an inexpensive, expendable mobile sound source was deployed to investigate potential use of such a device to acquire quality transmission loss (TL) data and yield additional spatial information of the complex acoustic environment. The mobile source was programmed to maintain depth, speed, and to transmit a tonal signal followed by a short linear-sweep timing/ranging pulse every minute. A vertical hydrophone array and other receivers recorded the signals. The methodology and related mathematical tools to analyze the received acoustic data for coherence time (optimum integration time) and consequently TL were developebcd. Specifically, coherence times were estimated based on a tolerance of one-dB degradation in the measured SPL of the tone. It is shown that a time segment is coherent when 50% of the segment has phase fluctuations within ± 45° about the linear trend of the phase. The optimum integration time was applied to the data to obtain TL estimates versus range using spectral estimation techniques. Measured coherence time and TL were compared to model results from the National Taiwan University to gain insights into the quality, limitations, and attainable future advances of this measurement method.

14. SUBJECT TERMS	**15. NUMBER OF PAGES**
South China Sea, mobile acoustic source, transmission loss, coherence time	51
	16. PRICE CODE

17. SECURITY CLASSIFICATION OF REPORT	**18. SECURITY CLASSIFICATION OF THIS PAGE**	**19. SECURITY CLASSIFICATION OF ABSTRACT**	**20. LIMITATION OF ABSTRACT**
Unclassified	Unclassified	Unclassified	UU

NSN 7540–01-280-5500 Standard Form 298 (Rev. 2–89)
Prescribed by ANSI Std. 239–18

THIS PAGE INTENTIONALLY LEFT BLANK

Approved for public release; distribution is unlimited

MEASUREMENT OF TRANSMISSION LOSS USING AN INEXPENSIVE MOBILE SOURCE ON THE UPPER SLOPE OF THE SOUTH CHINA SEA

Samuel W. Graessle
Lieutenant, United States Navy
B.S., United States Naval Academy, 2009

Submitted in partial fulfillment of the
requirements for the degree of

MASTER OF SCIENCE IN PHYSICAL OCEANOGRAPHY

from the

NAVAL POSTGRADUATE SCHOOL
September 2015

Author: Samuel W. Graessle

Approved by: Ching-Sang Chiu
Thesis Advisor

Chris Miller
Co-Advisor

Peter Chu
Chair, Department of Oceanography

THIS PAGE INTENTIONALLY LEFT BLANK

ABSTRACT

During the 2014 South China Sea Upper-Slope Sand Dunes Experiment, an inexpensive, expendable mobile sound source was deployed to investigate potential use of such a device to acquire quality transmission loss (TL) data and yield additional spatial information of the complex acoustic environment. The mobile source was programmed to maintain depth, speed, and to transmit a tonal signal followed by a short linear-sweep timing/ranging pulse every minute. A vertical hydrophone array and other receivers recorded the signals. The methodology and related mathematical tools to analyze the received acoustic data for coherence time (optimum integration time), and consequently, TL were developed. Specifically, coherence times were estimated based on a tolerance of one-dB degradation in the measured SPL of the tone. It is shown that a time segment is coherent when 50% of the segment has phase fluctuations within $\pm 45^{o}$ about the linear trend of the phase. The optimum integration time was applied to the data to obtain TL estimates versus range using spectral estimation techniques. Measured coherence time and TL were compared to model results from the National Taiwan University to gain insights into the quality, limitations, and attainable future advances of this measurement method.

THIS PAGE INTENTIONALLY LEFT BLANK

TABLE OF CONTENTS

THIS PAGE INTENTIONALLY LEFT BLANK

LIST OF FIGURES

LIST OF TABLES

THIS PAGE INTENTIONALLY LEFT BLANK

LIST OF ACRONYMS AND ABBREVIATIONS

CW	continuous wave
EMATT	expendable mobile acoustic training target
LFM	linear frequency modulated
MSP	mean square pressure
NTU	National Taiwan University
PSD	power spectral density
PSDE	power spectral density estimate
OMAS	OASIS mobile acoustic source
SMSP	signal mean square pressure
SMSPE	signal mean square pressure estimate
SNR	signal-to-noise ratio
SPL	sound pressure level
SCS	South China Sea
STD	standard deviation
TL	transmission loss
VLA	vertical line array

THIS PAGE INTENTIONALLY LEFT BLANK

ACKNOWLEDGMENTS

I would like to give a heartfelt thanks to my advisors, Professor Ching-Sang Chiu and Christopher Miller, for their continuous guidance and support.

THIS PAGE INTENTIONALLY LEFT BLANK

I. INTRODUCTION

A. BACKGROUND

The South China Sea (SCS) is an important operating area for the United States Navy. Trade worth an estimated value of $5.3 trillion passes through these waters every year (Glaser 2012). The United States has stated it intends to operate and ensure freedom of navigation is maintained in the SCS (Reuters 2015). To accomplish the mission, the Navy needs a firm understanding of the operating environment to properly tailor sensors and maintain tactical superiority. Detailed measurements of transmission loss (TL) of sound in the ocean can be costly and labor intensive to conduct. An inexpensive mobile source to measure TL of sound would greatly reduce cost and offer flexibility.

The 2014 South China Sea Sand Dunes Upper-Slope Sand Dunes Experiment was an Office of Naval Research and Taiwan Ministry of Science and Technology sponsored joint scientific experiment. The goals of the experiment were to examine the physics of sound propagation and associated variations in sound intensity due to nonlinear internal waves in a dune field (Miller et. al. 2014). The dunes lie along the upper continental slope of the SCS in water depth from 160 to 600 m with a material composition of primarily coarse to medium sand. The dunes have amplitudes up to approximately 16 m and crest-to-crest wavelengths longer than 200 m. Large nonlinear internal waves propagating across the basin of the SCS, originating at the Luzon Strait, are believed to factor into the formation of these sand dunes. Sound propagation in the ocean can be severely affected by how the sound propagates along the dunes (Reeder et. al. 2010).

The experiment was conducted over 18 days in this sand dune field. One component of the experiment focused on the deployment of an inexpensive mobile source acting as a sound transmitter. The mobile source was an Expendable Mobile Acoustic Training Target (EMATT) (Miller et. al. 2014). EMATTs are regularly used within the Navy as underwater training targets to simulate submarines. The EMATT was deployed from a ship and ran a programmed four km route from the northwest to the southeast past a hydrophone array mooring. Once at the two km radius from the mooring, the EMATT

completed two and half circle runs counterclockwise around the mooring. Finally, the EMATT conducted another pass of the mooring and ran out to sea. While transiting the route, the EMATT emitted sound signals on a one min duty cycle as delineated in Table 1. A vertical line array (VLA) hydrophone mooring recorded the sound pressure levels (SPL) at 173, 215, and 285 m water depth using an Acousonde® recorder manufactured by Acoustimetrics. Three additional moorings with hydrophone receivers were stationed in the sand dune field (Miller et. al. 2014). Figure 1 displays an overview of the EMATT experiment. The drop point for the EMATT is denoted and the black line represents the programmed track for the EMATT. The VLA is shown along with the three additional receivers, YS1, YS2, and CS1. The bathymetry is superimposed on the plot to show the sand dunes orientation.

Table 1. EMATT signal transmissions (after Miller et. al. 2014).

Transmission	Frequency	Duration	Source Level
Continuous Wave	1250 Hz	58 sec	150 dB
Linear Frequency Modulated	1250 – 3000 Hz	2 sec	Unknown

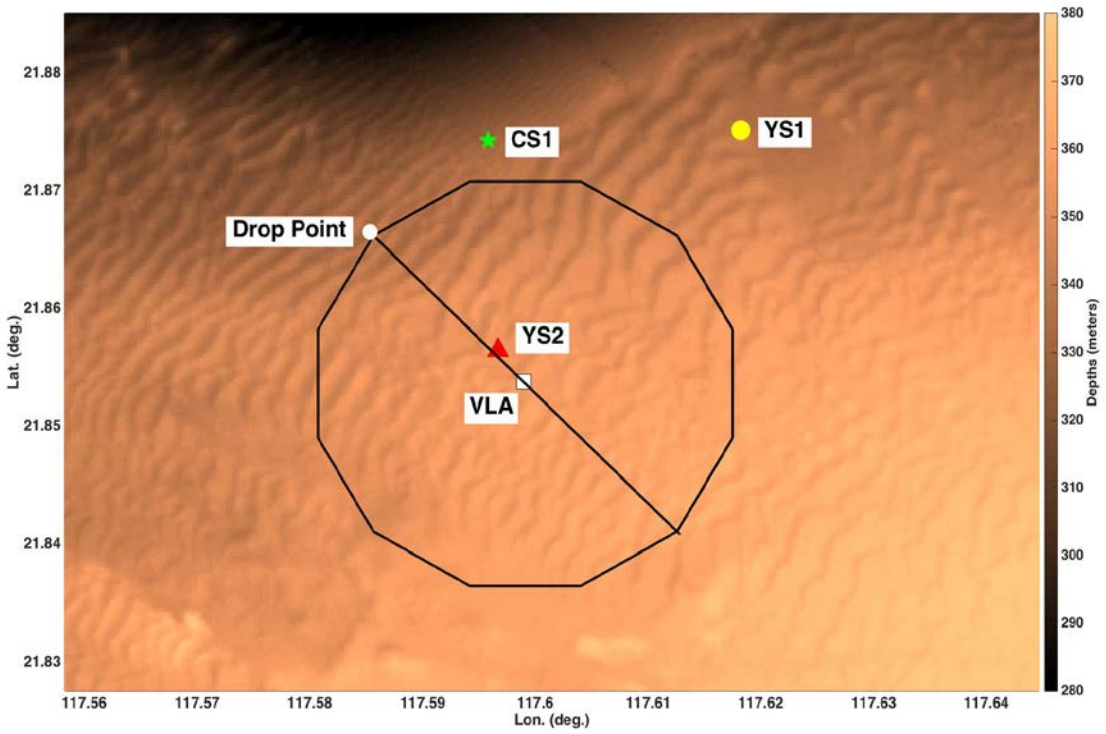

Figure 1. Location of VLA (white square), YS1 (yellow circle), YS2 (red triangle), and CS1 (green star) moorings and programmed track of EMATT superimposed on SCS bathymetry. EMATT drop point (white circle) is also shown (after Miller et. al. 2014).

B. PAST EMATT USE

This experiment was not the first time an EMATT has been used as an acoustic source for underwater acoustic measurements. OASIS Inc. built the OASIS mobile acoustic source (OMAS), a modified standard Navy issued EMATT, for use in in-situ acoustic measurement applications (Abbot et. al. 2006). The OMAS was modified with a precision clock allowing the vehicle to time synchronize with hydrophone receivers. This modification allowed for range calculation between source and receiver based on the time delay between signal and reception. The receivers also had a horizontal aperture that provided bearing to the OMAS. Additional modifications included a calibrated acoustic source programmed with longer programmable acoustic signal designs (Abbot et. al. 2006).

Previous OMAS deployments in shallow water used three acoustic waveform designs. The first was a hyperbolic frequency modulated slide. This signal was match filter processed for time delay to determine range and integrated to obtain TL. The second signal was a tone burst for Doppler and TL measurements and the third was a continuous wave (CW) signal for tracking, TL, and Doppler measurements. Using the calculated range and the bearing to the source from the directional receiver, an accurate track of the OMAS was able to be determined (Abbot et. al. 2006).

These OMAS experiments proved the feasibility of using EMATTs as mobile acoustic sources for underwater acoustic measurements, however they were done at an additional cost. The EMATTs were significantly modified from the standard Navy EMATT to serve this purpose. Modifications to the acoustic signal design and the addition of a precision clock greatly increased the price of an EMATT. The research in this thesis focuses on using an unmodified off-the-shelf standard issue Navy EMATT as a mobile acoustic source. Whereas past research has relied on directional receivers to provide bearing to the source, the work in this thesis uses dead reckoning from the initial drop point to build a range over time solution and moored receivers for localization.

C. OBJECTIVE

The objective of this research was to evaluate using a standard Navy EMATT as a mobile acoustic source for underwater acoustic measurements of TL. This required the development of appropriate methodology and analysis tools to process the collected data. Due to the unique and complex location of the experiment in the sand dune field, the EMATT was programmed to run geometries in relation to the sand dunes to provide insight into azimuthal and range effects on TL. Measured results compared with model results from the National Taiwan University (NTU) (Chen and Yeh 2015, personal communication) provide a consistency check between the two efforts.

D. APPROACH

Fundamental to an accurate estimation of TL is understanding the temporal and spatial coherence scale of the received signal. The amount of time that a reference acoustic signal can be considered coherent, i.e. the phase on average is predictable or

bounded, is the coherence time (NCSTSD 1996). The first step of this thesis was to estimate coherence time of the CW signal emitted by the moving source. This coherence time was then used as the integration time to calculate the SPL of the received signal and estimate TL. Using the initial starting point of the EMATT, a range over time solution for the EMATT was developed based on cross-correlation of the linear frequency modulated (LFM) sweep at the VLA. Additionally, a non-linear least squares solution based on time difference of arrivals between the three additional hydrophones was developed to assess the location of the EMATT. Coherence time and TL-versus-range measurements derived from the EMATT were compared to model results.

E. THESIS OUTLINE

This thesis contains three chapters following the introduction. Chapter II describes the methodology used to estimate coherence time and TL. Chapter III gives a discussion of the data analysis results for measured coherence time, source positions, measured TL, and a comparison of the modeled results to measured results. Finally, conclusions and recommendations are provided in Chapter IV.

THIS PAGE INTENTIONALLY LEFT BLANK

II. METHODOLOGY

A. TRANSMISSION LOSS

Transmission loss, TL, is the reduction of SPL in dB as sound travels from a source to a receiver (Urick 1983). The basic equation to obtain TL from measurements in a tonal transmission is:

$$TL = SL - SPL \tag{2.1}$$

where *SL* is the known source level (in dB). *SPL* is the sound pressure level in dB, measured at the receiver. TL is attributed to the sum of losses due to spreading, multipath effects, scattering, and attenuation (Urick 1983). Typical values for TL in different areas of the ocean are important for the Navy to know in order to properly tailor sensors and know the best location to position them. SPL is a logarithmic measure of the signal mean square pressure (SMSP) (Clay and Medwin 1977):

$$SPL = 10\log\frac{SMSP}{1\,\mu Pa^2} \quad re\,1\,\mu Pa \tag{2.2}$$

In this experiment, a time series of sound pressure data was obtained. The processes to analyze the data to calculate SMSP and TL have been developed as part of this thesis.

In a static, no-noise environment with a fixed source and fixed receiver, a time series of received pressure data can be integrated over one period of the signal to give the SMSP (Clay and Medwin 1977):

$$SMSP = \frac{1}{T}\int_0^T p(t)^2\,dt \tag{2.3}$$

In reality, the ocean is not static and a multitude of factors influence the signal as it travels from the source to receiver. Relative motion between the source and receiver, Doppler phase shift, and ocean waves (tidal, sub-tidal, solitary internal waves, sea surface roughness) each cause signal path amplitude and phase fluctuations. There is also random noise that contaminates the signal (Clay and Medwin 1977). To determine the SMSP in a real-world environment, measures have to be taken to ensure it is a reliable estimate.

Calculation of received SMSP can occur in the time domain or frequency domain in accordance with Parseval's Theorem. Calculation of energy in the frequency domain allows for easier integration over frequencies of interest than working in the time domain (Emery, Thompson 2004). By looking at the power spectrum of a time series, we are able to characterize the received amplitudes or pressures as a function of frequency. From Bendat and Piersol (1971), if power spectral density "is estimated by direct Fourier transform operations… a smoothing operation must be performed to ensure a consistent estimate". The smoothing operation can be accomplished by smoothing over an ensemble of the estimates or by smoothing over frequency. Both processes produce consistent estimates (Bendat and Piersol 1971). Single sided power spectral density estimates (PSDE) for this research were smoothed over frequency as defined by:

$$\widehat{G}_{pp}(f,B) = \frac{2}{TB}\int_{f-B/2}^{f+B/2} \left|P(f')\right|^2 df' \tag{2.4}$$

The frequency smoothing bandwidth, *B*, is the resolution of the PSDE. From Bendat and Piersol (1971), the normalized standard error that characterizes the random portion of the estimation error, $\in$, is:

$$\in = \frac{\sigma\left[\left|\widehat{G}_{pp}(f,B)\right|\right]}{\left|G_{pp}(f,B)\right|} = \frac{1}{\sqrt{BT}} \tag{2.5}$$

To ensure a statistically reliable $\widehat{G}_{pp}(f,B)$, a maximum normalized standard error of 10% was desired. This dictated the size of the frequency smoothing bandwidth and minimum integration time required.

After a statistically reliable estimate for power spectral density (PSD) has been made, the spectrum is integrated over a frequency band centered on the signal frequency to estimate the signal-plus-noise mean square pressure. The PSD is then integrated again over an adjacent frequency band to estimate the in-band noise. Using the equation below, the noise mean square pressure estimate is subtracted from the estimate for signal-plus-noise to estimate the signal mean square pressure.

$$SMSPE = \int_{f_o - B/2}^{f_o + B/2} \hat{G}_{pp}(f, B)df - \int_{f_o + B/2}^{f_o + 3B/2} \hat{G}_{pp}(f, B)df \tag{2.6}$$

The final step for reliability is to determine the length of the time series to be used for integration. The minimum integration time length is determined by the requirement for a maximum normalized standard error of 10% in the PSDE. The maximum integration time is determined by the coherence of the signal.

In the presence of white, Gaussian random noise, the longer the integration time, the higher the signal-to-noise ratio (SNR) so long as the signal remains coherent. When calculating the received SMSPE, the estimate will continue to increase until the coherence time of the signal has been reached, after which the SMSPE level will taper off. Thus a signal's optimal integration time is the maximum length of time over which a CW signal remains coherent. This time needs to be determined so that measured estimates of SMSP are all optimal estimates, measured over coherent signal lengths.

B. SIGNAL MODEL

A one dB degradation in the SMSPE was used in this study to characterize the limiting time duration in which the signal is coherent and any further integration of the signal would not yield an increase in received energy. A signal model, *p(t)*, of received pressure was developed for Monte Carlo simulation of the received signal, allowing for the evaluation of various effects on the signal and which effect would lead to a one dB degradation in SPL. The signal used can be express as:

$$p(t) = \left(\frac{A_o r_o}{r} + \delta A\right)\sin\left(2\pi f_o t + \frac{\nu}{c} f_o t + \delta\theta\right) \tag{2.7}$$

where *p(t)* is the acoustic pressure at the receiver, A_o is amplitude of the tone at r_o where r_o is one m, r is the source-to-receiver range, δA represents random amplitude fluctuations, f_O is acoustic frequency, t is time, $\frac{\nu}{c} f_o$ represent Doppler effects, and $\delta\theta$ represents random phase fluctuations.

The first time series simulated was the baseline to simulate a signal traveling from a fixed source to a fixed receiver in an ideal static environment. It neglected any amplitude changes or Doppler effects due to relative motion between source and receiver and did not take into account random amplitude fluctuations or random phase fluctuations caused by the environment. A PSD estimate was made of the simulated time series and the mean square pressure (MSP) was calculated over a frequency band. By comparing the overall MSP as additional effects influenced the signal, the effects causing a one dB decrease in SPL estimate could be singled out. Figure 2 shows the baseline pure signal and three simulated effects on the signal.

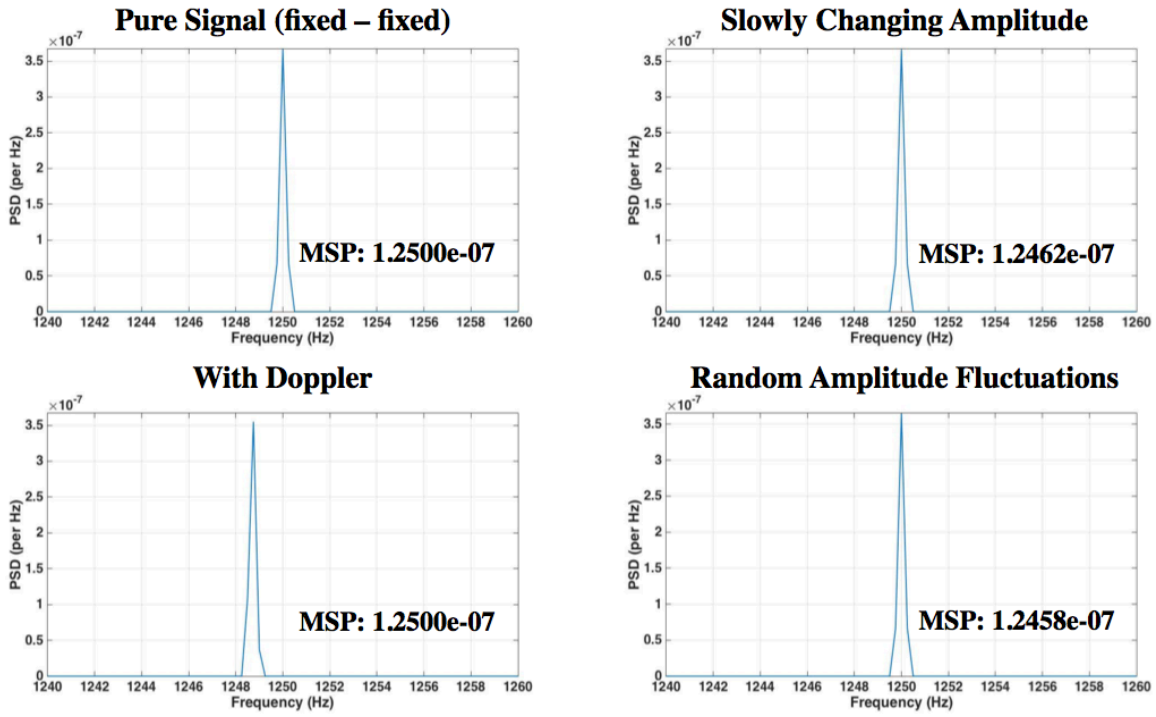

Figure 2. Power spectral density plots and mean square pressure estimates of simulated signals for a pure signal for fixed source and fixed receiver, (top, left); with slowly changing amplitude effects (top, right); with Doppler effects (bottom, left); and with random amplitude fluctuations (bottom, right).

The top left quadrant of Figure 2 is the baseline PSD and MSP for the pure signal from a fixed source to a fixed receiver. The top right quadrant of Figure 2 is a plot of the

PSD and calculated MSP estimate for the signal incorporating slowly changing amplitude effects that would be caused by range variation between source and receiver. The received MSP estimate had a negligible decrease compared with received MSP of the pure signal. The bottom left quadrant of Figure 2 displays the received MSP estimate of the signal incorporating Doppler effects resulting from relative motion between source and receiver. Doppler effects only result in a frequency shift at the receiver; not to any decrease in the MSP estimate. Doppler shifts are not a factor because all of the energy can be captured by properly selecting the signal integration band. The bottom left quadrant in Figure 4 displays the PSDE and MSP estimate of the signal influenced by random amplitude fluctuations caused by inhomogeneity in the sound channel and uncertainties in the range and depth of the source. The random amplitude fluctuations, δA, were modeled to have a normal distribution with a standard deviation (STD) that is 50% of the unperturbed amplitude. Random amplitude fluctuations did not have a significant effect on the received MSP estimate and therefore were not a determining factor in degradation of the SPL estimate.

Finally, the effects of random phase fluctuations on the signal were modeled. Environmental effects and platform motion of the receiver and source induced random phase fluctuations in the signal. Random phase fluctuations, $\delta\theta$, were first simulated by a normal distribution with a STD of 33°. This yields a distribution with 50% of the phase fluctuations between ± 22.5° of the mean phase. The results are displayed in Figure 3.

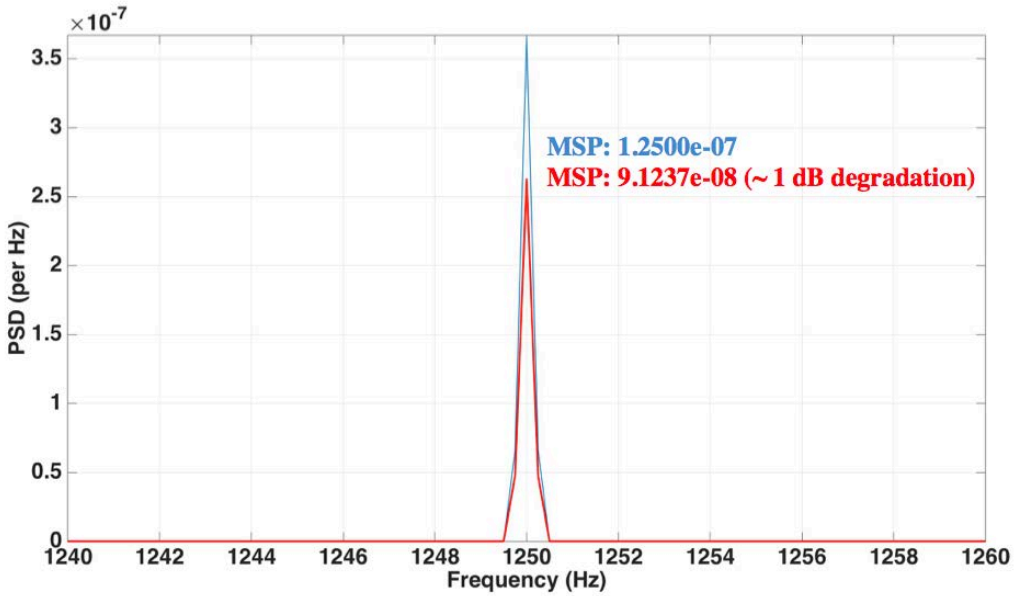

Figure 3. Power spectral density plots and mean square pressure estimates for simulated pure signal, fixed source fixed receiver (blue); and with random phase fluctuations based on a normal distribution with an STD of 33° (red).

Random phase fluctuations based on a normal distribution resulted in a degradation of approximately one dB in the SPL estimate. The same effect of random phase fluctuations was then modeled using a uniform distribution with phase fluctuations between ± 45°, also yielding 50% of the phase fluctuations between ± 22.5° of the mean phase. The results are displayed in Figure 4.

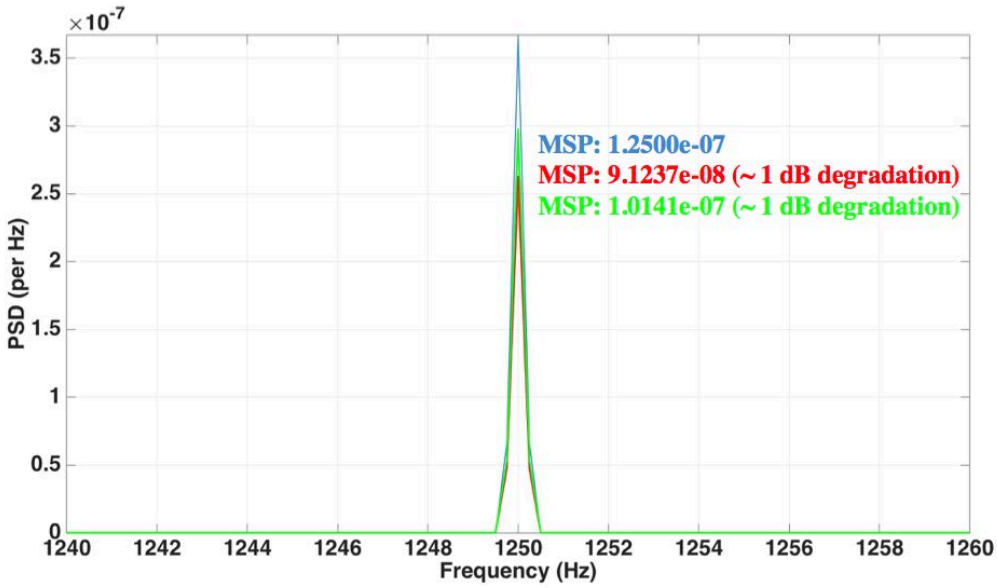

Figure 4. Power spectral density plots and mean square pressure estimates for simulated pure signal, fixed source fixed receiver (blue); random phase fluctuations based on a normal distribution with an STD of 33° (red); random phase fluctuations based on a uniform distribution between ± 45° (green).

Random phase fluctuations that fell within a uniform distribution between ± 45° also lead to a degradation in SPL of approximately one dB. When phase fluctuations were modeled to have normal and uniform distributions where phase fluctuations were between ± 22.5°, there was the same approximate one dB degradation to SPL. The effects of more severe random phase fluctuations were then modeled, first with random phase fluctuations between ± 90°, and then completely random between ± 180° as shown in Figure 6.

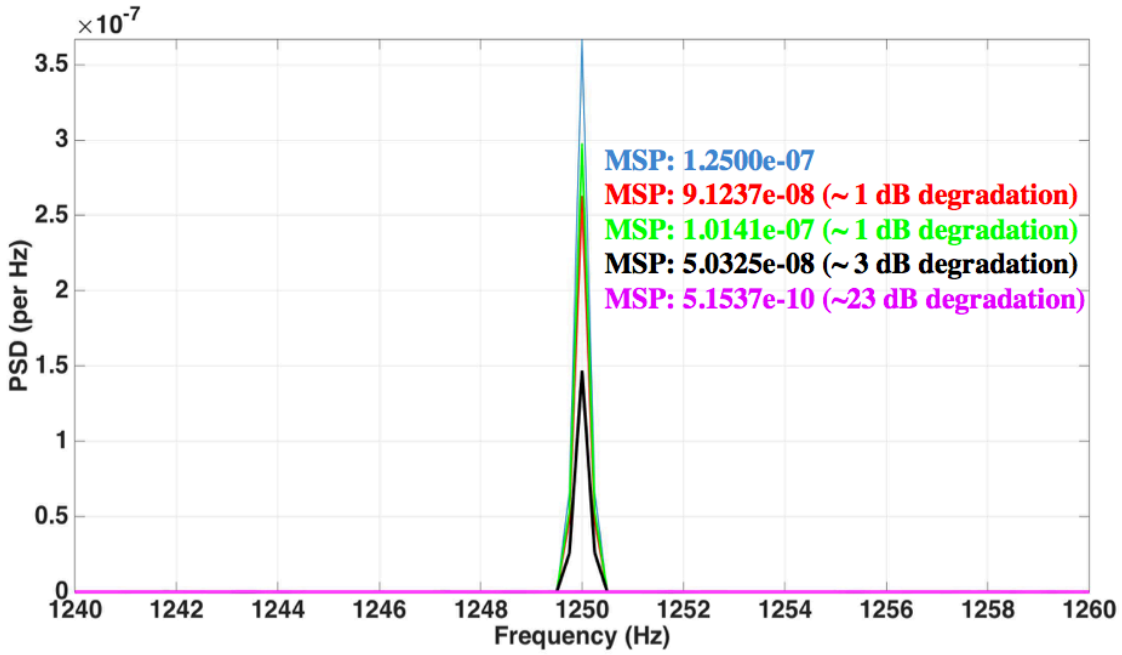

Figure 5. Power spectral density plots and mean square pressure values for simulated pure signal, fixed source fixed receiver (blue); random phase fluctuations based on a normal distribution with an STD of 33° (red); random phase fluctuations based on a uniform distribution between ± 45° (green); random phase fluctuations based on a uniform distribution between ± 90° (black); random phase fluctuations based on a uniform distribution between ± 180° (purple).

Random phase fluctuations that fell between ± 90° lead to a decrease in the SPL estimate of approximately three dB. Once the random phase fluctuations became completely random and varied from ± 180° , the received signal became completely lost in the noise. From this signal model, it was determined that random phase fluctuations are the main cause for signal incoherence. When over 50% of the random phase fluctuations were outside a 45° quadrant (± 22.5°), the signal became incoherent and had a greater than one dB degradation in SPL.

III. DATA ANALYSIS

A. COHERENCE TIME

Using the tools developed in the methodology section, coherence time was calculated from the data. The CW tonal provided 58 sec of data for each minute. This data was segmented into four 20 sec periods of data to increase the number of realizations. SMSP estimates for the signal were made with a minimum integration time of four sec and a frequency bandwidth of 25 Hz centered on the 1250 Hz signal. This met the 10% normalized standard error requirement. The integration time was then increased incrementally up to the maximum time of 20 sec. As the integration time increased, the normalized standard error for the estimate decreased. SMSP and SPL estimates as a function of integration time were calculated. The point at which the SPL estimate degraded by one dB from the maximum determined the coherence time. Figure 6 displays an example of one realization. In this case, the coherence time was 10 sec.

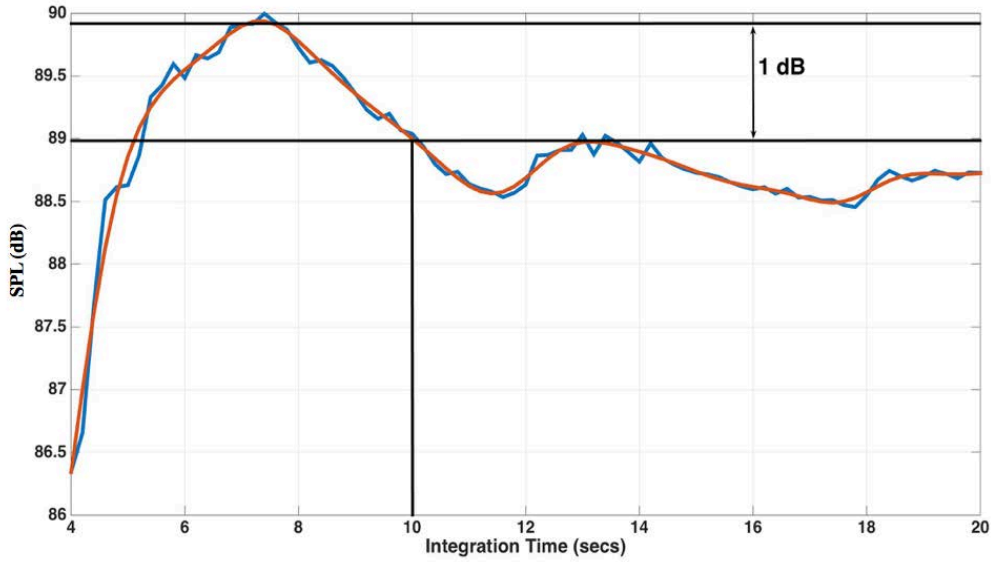

Figure 6. Power spectral density estimate vs. integration time. The time at which the SPL estimate suffers a 1 dB decrease defines the coherence time for this particular transmission.

This process was applied to the entire data set to increase the number of realizations for coherence time. Figure 7 displays coherence time over the time the EMATT was deployed.

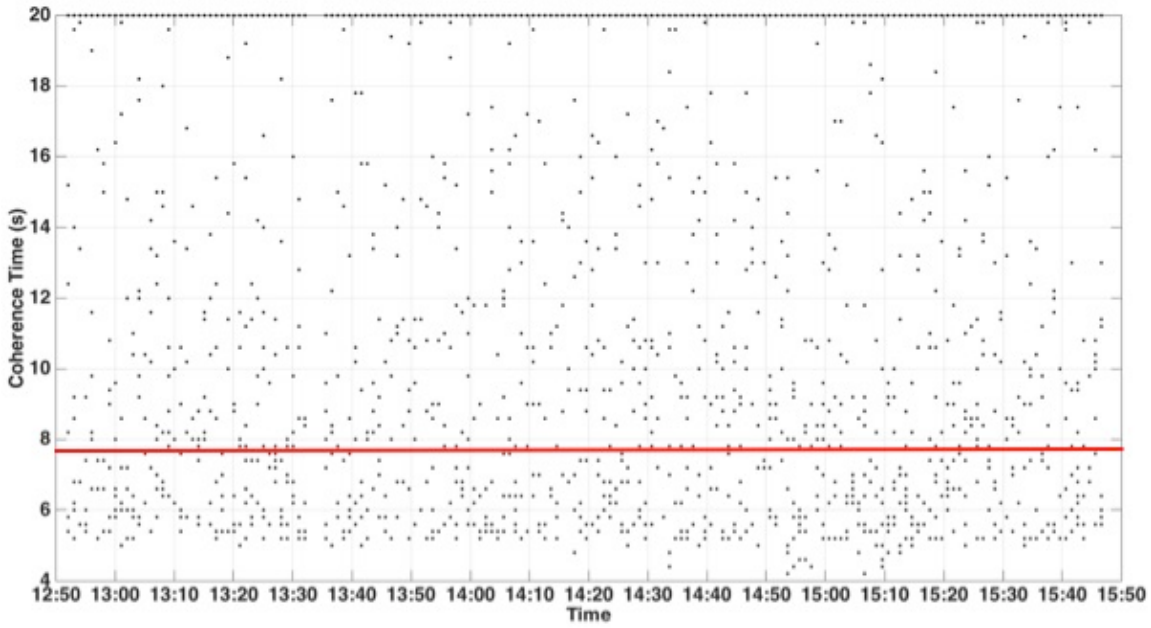

Figure 7. Coherence time in seconds over time EMATT was deployed.

There were no distinguishing trends in coherence time as the EMATT attempted to follow its programmed route. There were a large number of realizations at 20 sec for coherence time. This means that the coherence time for those transmissions was at 20 sec or greater since no integration times were calculated for longer than 20 sec. Because of this fact, the coherence time estimate is conservatively biased. It would be difficult to estimate different coherence times for transmission loss calculations based on source bearing and range so one standard coherence time was chosen. A mean of the coherence time estimates, less one standard deviation was used as optimal integration time for TL estimates. This gave a conservative estimate and ensured that a long enough integration time to optimize SNR and prevent degradation.

B. SOURCE POSITIONS

After the optimal integration time was determined for transmission loss calculations, a range profile of the EMATT over time was developed. The two sec LFM sweep following the 58 sec tonal was used for ranging and tracking purposes. The arrival of the LFM sweep was cross-correlated at the VLA to determine relative time of arrival of the sweep for each minute. Based on the relative time difference of arrival between successive minutes, the corresponding change in range between adjacent minutes was computed. Adding the initial range gave the range of the EMATT as a function of time. Range vs. time is shown in Figure 8.

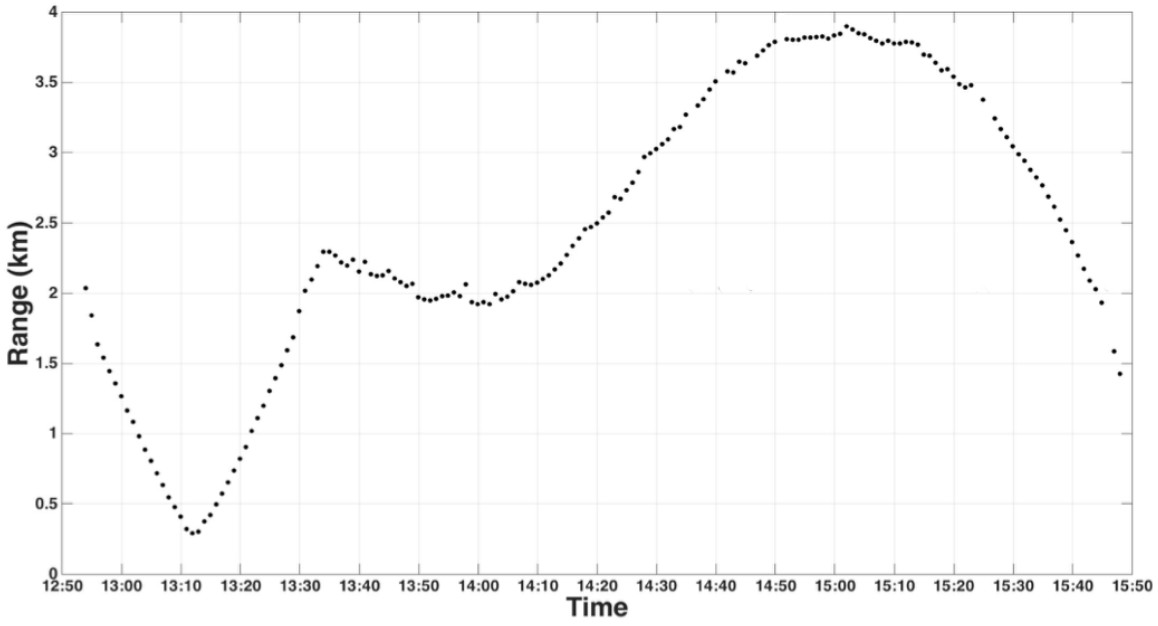

Figure 8. Plot of EMATT range (km) from VLA over time.

Based on results of the EMATT range from VLA over time, it can be seen that the EMATT initially follows the programmed route well. The range decreases from two km until the closest point of approach with the VLA at approximately 290 m. The spacing between the arrivals on the initial leg indicates that the EMATT was approaching and leaving the VLA as expected. The EMATT then proceeded past the VLA as planned out to approximately two km where it was programmed to start a counter-clockwise circular

track. At this point in time, it was expected for the range to stay relatively constant at two km as the EMATT attempted to complete the circle. It is clear from the results that the EMATT initially started out following the circle but then was caught up in strong currents that took it off course. From the sine-wave nature of the remaining portion, it is estimated the EMATT did continue to attempt its programmed circular route, however it was no longer centered on the VLA once it was pushed off track by the currents.

Following the indications that the EMATT was pushed off track, an effort was made to estimate the actual position of the EMATT. The LFM sweep of the EMATT was used again for position estimation by cross-correlating the sweep arrival at the three additional hydrophone moorings. The sweep arrival times from each receiver were then used to calculate the time difference of arrival between the receivers. Using three time differences of arrival, an estimate for the EMATT position could be made. This is only possible with sufficient SNR that the LFM sweep is detectable at all three receivers. Due to bandwidth constraints on the LFM sweep because of concurrent transmission experiments in the vicinity, SNR of the sweep was not high enough on all three receivers at the same time for more than a few minutes. This allowed for a positional estimate of the EMATT for only a small fraction of time. Figure 9 displays a positional estimate of the EMATT when SNR was sufficient at all three receivers.

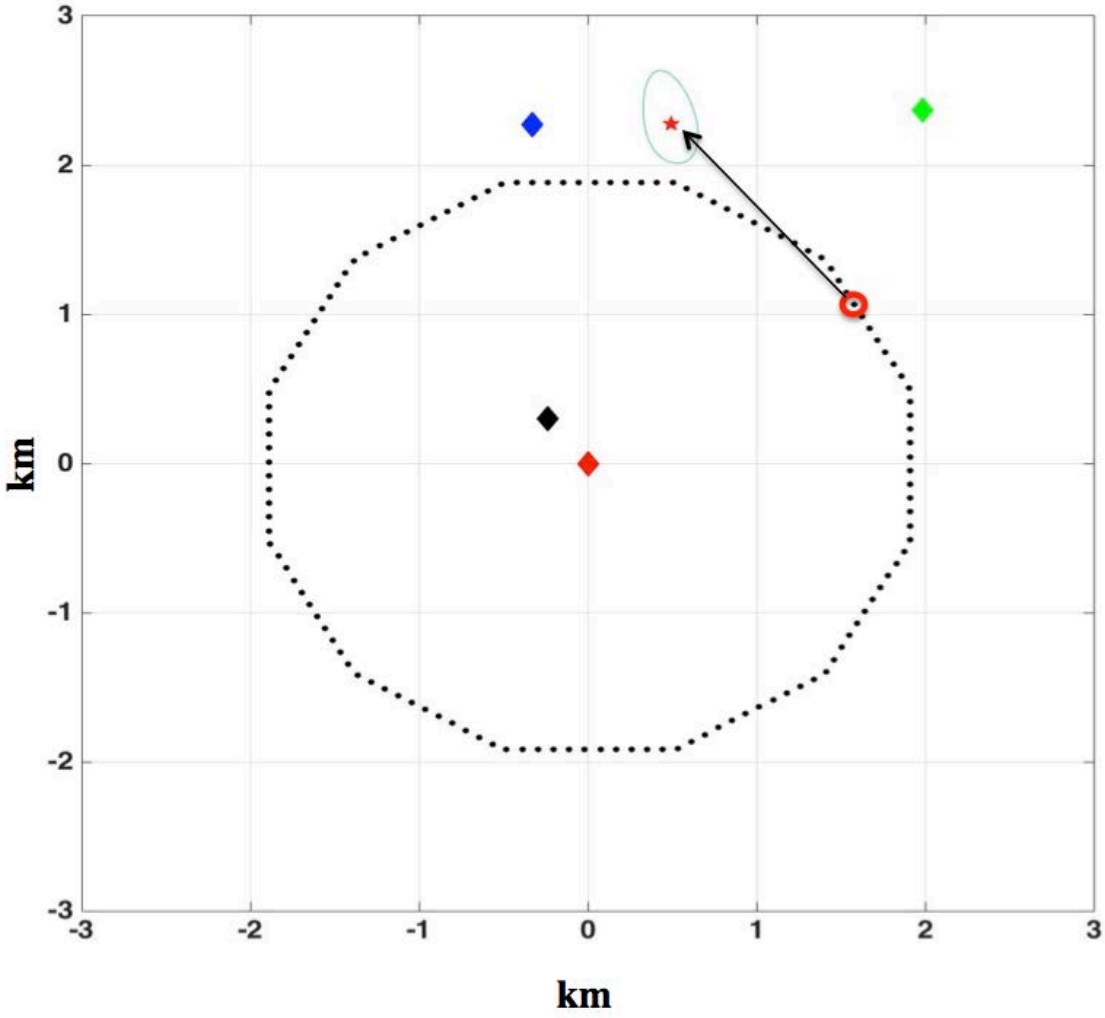

Figure 9. Estimated position of EMATT (red star) based on time difference of arrivals between three SHRUs (blue, green, and black diamond). Black dots are programmed track for EMATT and the red circle indicates intended position for EMATT at time of position estimation. Light blue line represents uncertainty of the EMATT position estimation due to multipath arrival spread.

From Figure 9, the EMATT was pushed off course to the northwest. The red star represents the non-linear least squares position solution, calculated from the measured time differences of arrival from the cross-correlation of the hydrophone data. With a multipath arrival spread of approximately 15 ms in the time difference measurements, an error estimate in range was also computed denoted by the blue circle. It is possible the EMATT is located anywhere inside the blue circle at that time. Due to lack of SNR to estimate EMATT position over the entire deployment and the degree of uncertainty

associated with the positional estimates, all TL estimates were made solely as a function of range with no bearing information, except when the EMATT was moving on the initial straight line path.

C. TRANSMISSION LOSS

To calculate TL, the 58 sec CW tonal pressure data was broken down into segments and integrated using the 7.8 sec optimal integration time. This provided six realizations of TL for each minute of data. TL as a function of range was calculated for the Acousonde® receivers at 185, 215, and 285 m depths on the VLA. Figure 10 displays the results of TL over range for the receiver at 173 m depth.

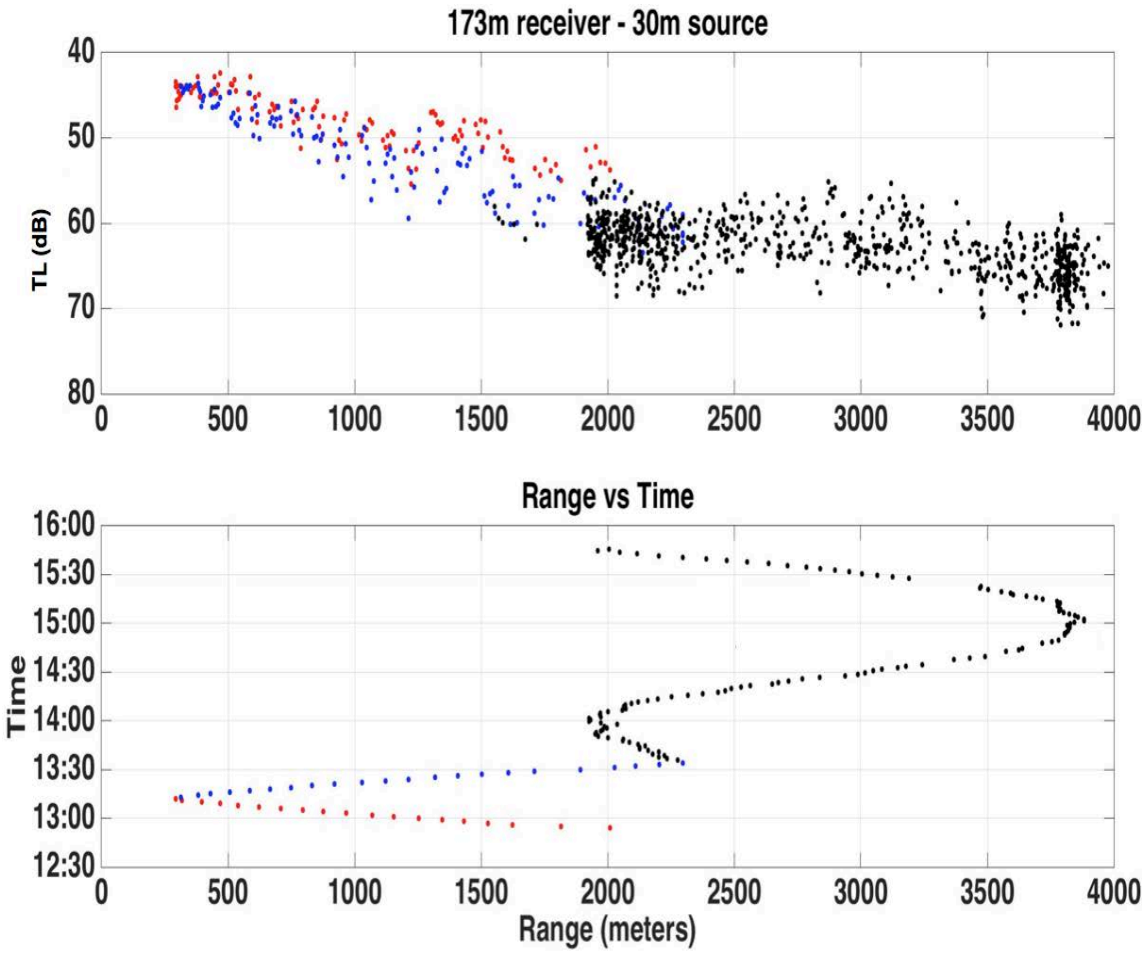

Figure 10. Upper panel shows the estimated TL-versus-range for source at 30-meter depth and receiver at 173 m depth. Red dots denote TL estimate as EMATT on heading 135 approaching VLA, blue dots denote TL estimate as EMATT on heading 135 leaving VLA, and black dots denote TL estimate as EMATT was attempting the programmed circular track. The lower panel shows EMATT range from VLA as function of time. Red dots denote EMATT is on heading 135 approaching VLA, blue dots denote EMATT is on heading 315 leaving VLA, and black dots denote EMATT was attempting the programmed circular track.

From the results, there is clear evidence of two different slopes for TL. The first slope starts at the closest range of 290 m and proceeds out to two km. Once at the two km mark, there is a shift to a more gradual slope. The initial slope is likely spherical spreading and the second slope represents a shift to cylindrical spreading. There is also

evidence of sound convergence at approximately the 1500-1800 m range as indicated by the lower loss features at those ranges.

Figure 11 displays the results of TL over range for the receiver at a 215 m depth.

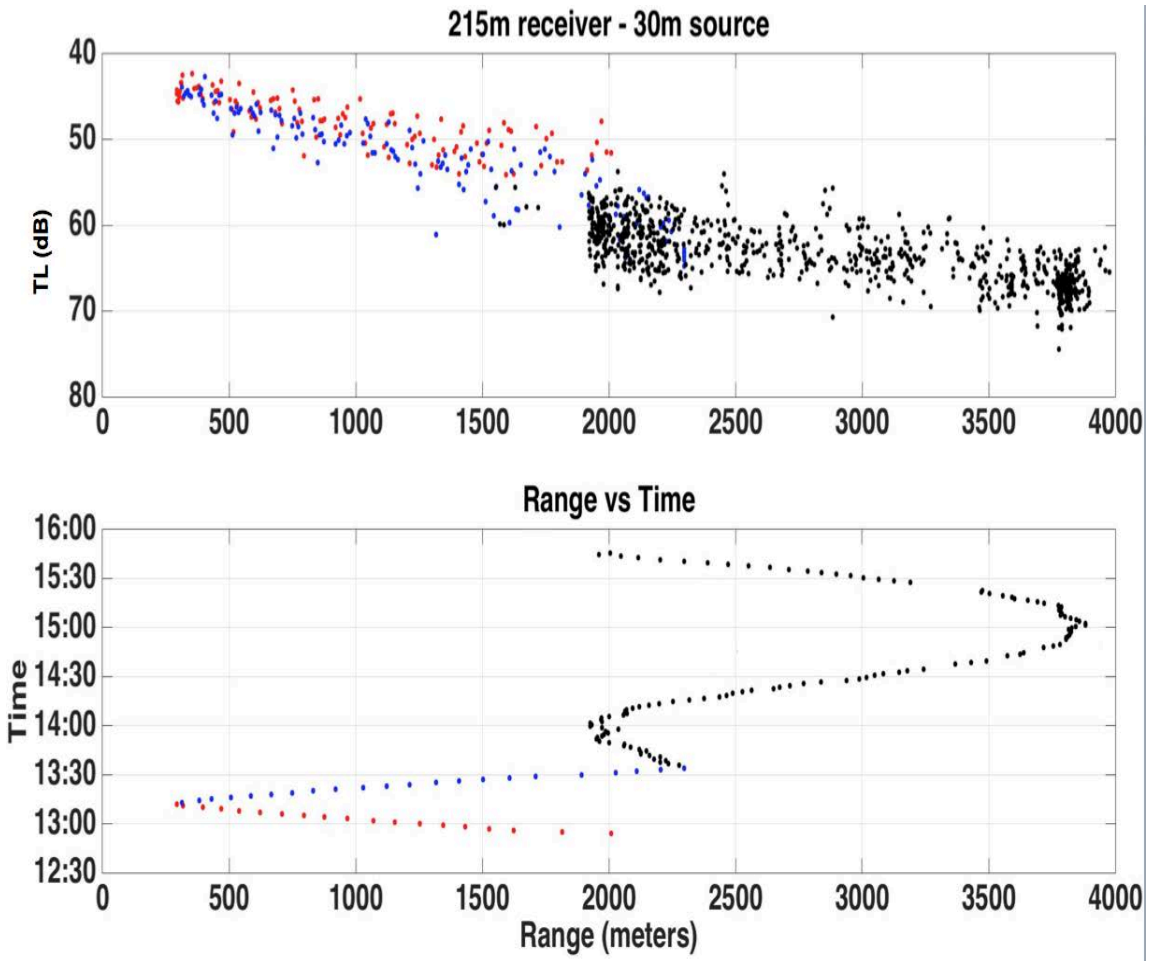

Figure 11. Upper panel shows the estimated TL-versus-range for source at 30-meter depth and receiver at 215 m depth. Red dots denote TL estimate as EMATT on heading 135 approaching VLA, blue dots denote TL estimate as EMATT on heading 135 leaving VLA, and black dots denote TL estimate as EMATT was attempting the programmed circular track. The lower panel shows EMATT range from VLA as function of time. Red dots denote EMATT is on heading 135 approaching VLA, blue dots denote EMATT is on heading 315 leaving VLA, and black dots denote EMATT was attempting the programmed circular track.

Similar to the shallower receiver, there are two distinct slopes for TL at the 215 m receiver depth as caused by spherical and cylindrical spreading.

Figure 12 displays the results of TL over range for the receiver at a 285 m depth.

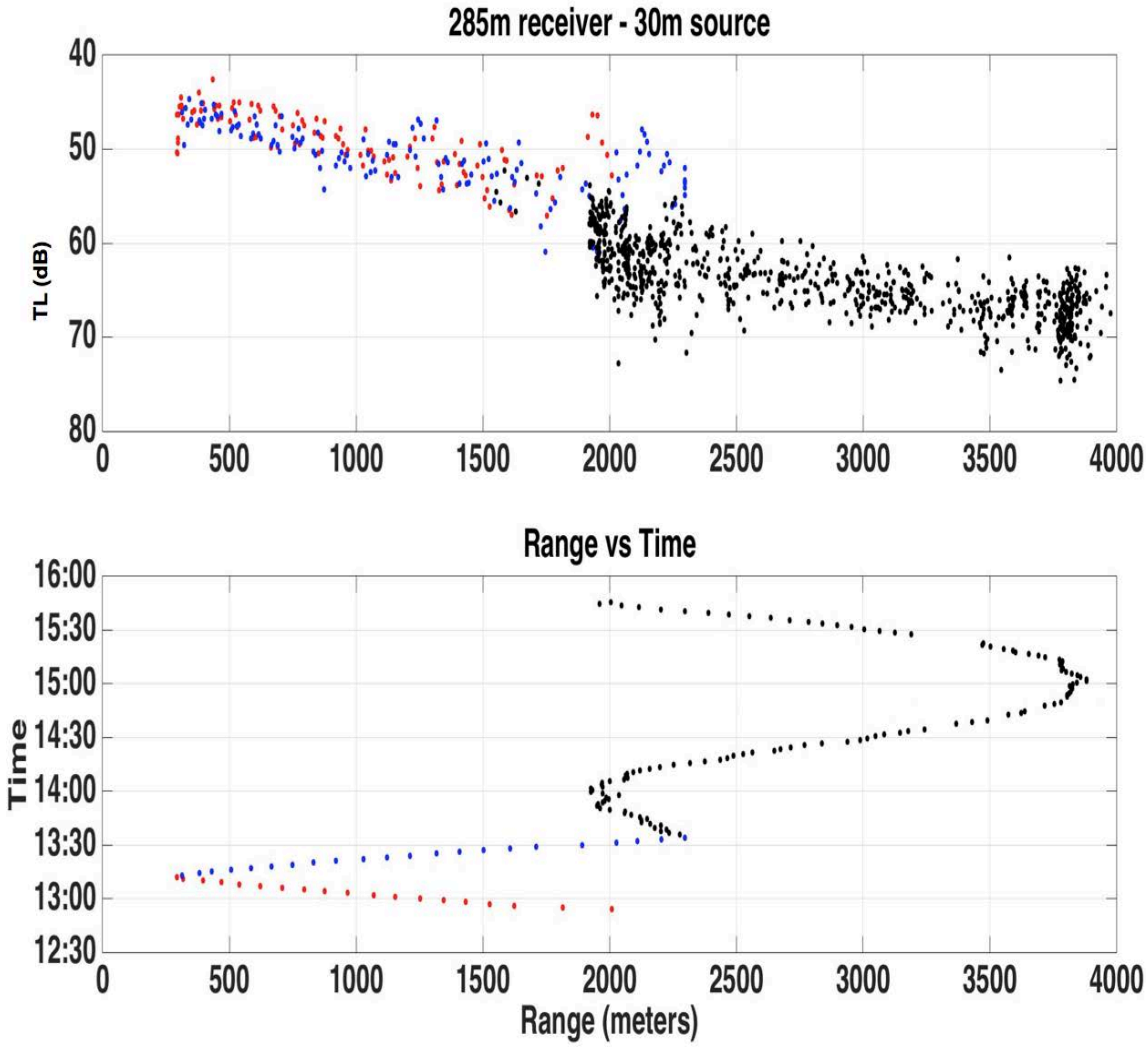

Figure 12. (Upper) TL (dB) versus range for source at 30-meter depth and receiver at 285-meter depth. Red dots indicate TL as EMATT is on heading 135 closing VLA, blue dots indicate TL as EMATT is on heading 135 opening VLA, and black dots indicate TL as EMATT is on programmed circular track. (Lower) EMATT range from VLA (meters) as function of time. Red dots indicate EMATT is on heading 135 closing VLA, blue dots indicate EMATT is on heading 135 opening VLA, and black dots indicate EMATT is on programmed circular track.

At the 285 m depth receiver, there are also two different slopes for TL. This is a commonality at all three depths. The lack of depth dependence on TL is likely due to the shallow depth of the source, 30 m, during these TL measurements. The receivers were capturing the same rays from the source, surface-reflected bottom-reflected rays. Refracted bottom-reflected rays did not reach the receivers that were at lower depths.

D. MODEL-DATA COMPARISON

In conjunction with the actual measured results of coherence time and transmission loss, Chen and Yeh (2015) developed a model for coherence time and transmission loss. The model was based on a range dependent parabolic equation model (Chen and Yeh 2015, personal communication). The goal was to make comparisons between the modeled coherence time and TL to support the measured results and vice versa. The modeled coherence time calculations were based on the metric that the signal was incoherent when 50% of the phase fluctuations in the time segment had deviated more than 22.5° from the linear trend. The model calculated coherence time up to a maximum of 60 sec. Coherence time was first modeled to simulate the initial leg of the EMATT. The model simulated coherence time along the 315° radial and 135° radial from 0-4,000 m in each direction. The modeled coherence time results as a function of horizontal range from the receiver are displayed in Figure 13.

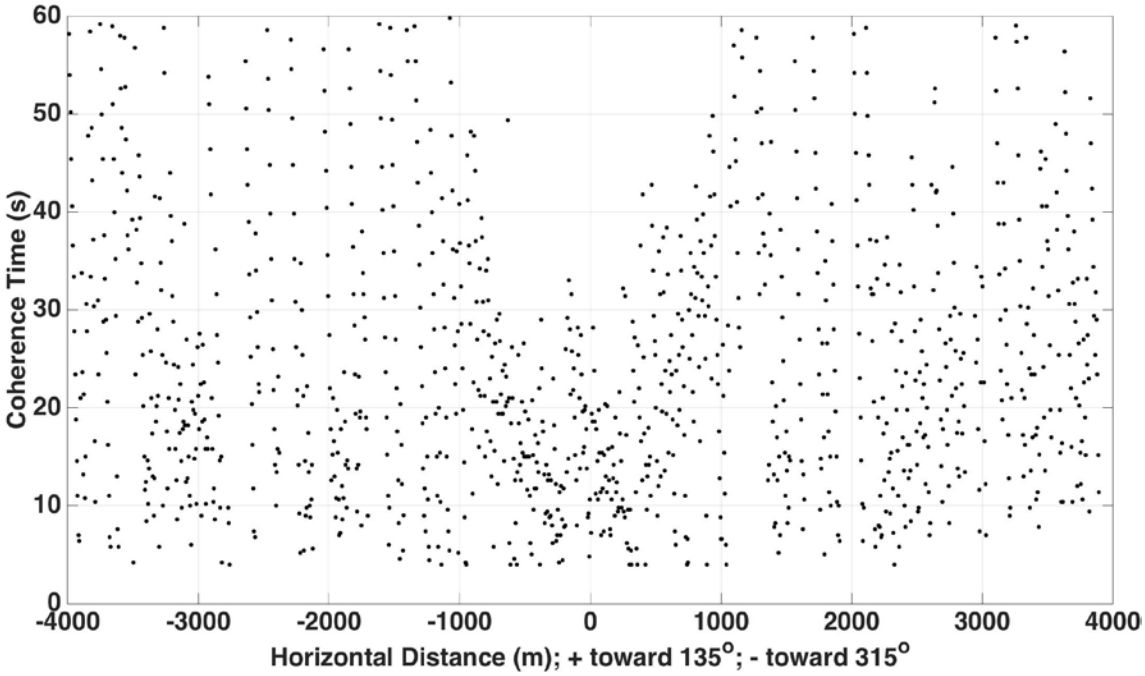

Figure 13. Modeled coherence times as a function of horizontal distance. Positive distances are towards the 135° radial and negative distance are towards the 315° radial. Source at 30 m depth, receiver at 285 m depth. (from Chen and Yeh 2015, personal communication)

From the model results there is a clear range dependence on coherence time. The coherence time is longer at distances further from the receiver and shorter when the source is closer to the receiver. This is intuitive due to strong changes in the multipath effects at the receiver as the source gets closer. The closer the range, the multipaths that interfere are more significant. The model results are from pure environmental effects and do not take into account any variations in the source's speed, depth, and heading changes. It should be noted that the modeled range dependencies of coherence time are greater than 20 sec. With the data coherence time measurements limited to 20 sec as shown previously in Figure 7, range dependence was not observable. Similarly, coherence time was then modeled as function of angle from the receiver with the source at 2 km. Figure 14 shows the model's calculated coherence time for the 2 km radius circle.

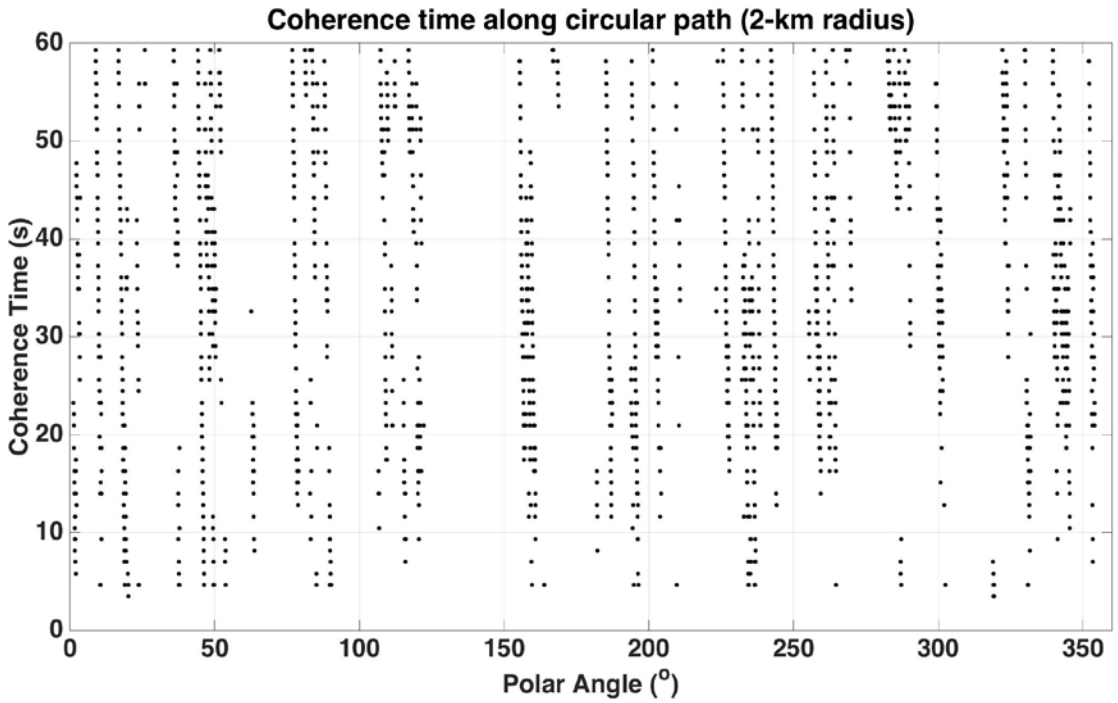

Figure 14. Modeled coherence times as a function of polar angle from the receiver. Source at 30 m depth, 2 m radius; receiver at 285 m depth. (from Chen and Yeh 2015, personal communication)

Coherence time is longer at some bearings and shorter at others. If coherence time was longer than 60 sec it was not plotted. The longer coherence times are realized when the transmission paths are oriented orthogonal to the sand dune crests, along the wider sand dune troughs, and toward sectors of relatively flat bathymetry. As the source moves around the circle, the change in bathymetry with respect to bearing is significant. For example, when the transmission paths are oriented along or diagonally to the sharp sand dune crests, the coherence time is significantly shortened.

TL was modeled as a function of horizontal range out to 4000 m from the receiver along the 135° and 315° radials. The source was at a 30 m depth and the receiver at 285 m depth. The model results along these radials is plotted with all measured TL vs. range, even though the measured results greater than two km are known to not lie along these radial tracks. They have been included to show the general agreement between measured and modeled results in this environment. Figure 15 displays the model results along the 135° radial and Figure 16 displays the model results along the 315° radial.

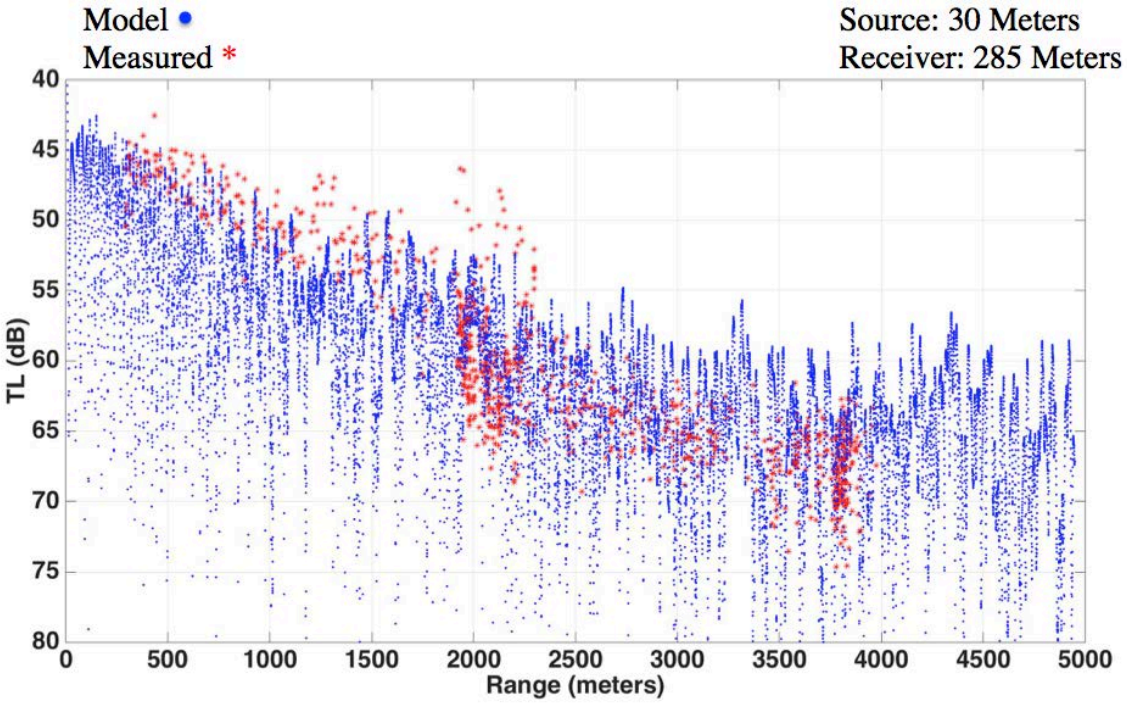

Figure 15. Modeled TL results along the 135° radial (blue dots) and measured TL results (red stars) as a function of horizontal distance from receiver. Source at 30 m depth, receiver at 285 m depth (after Chen and Yeh 2015, personal communication).

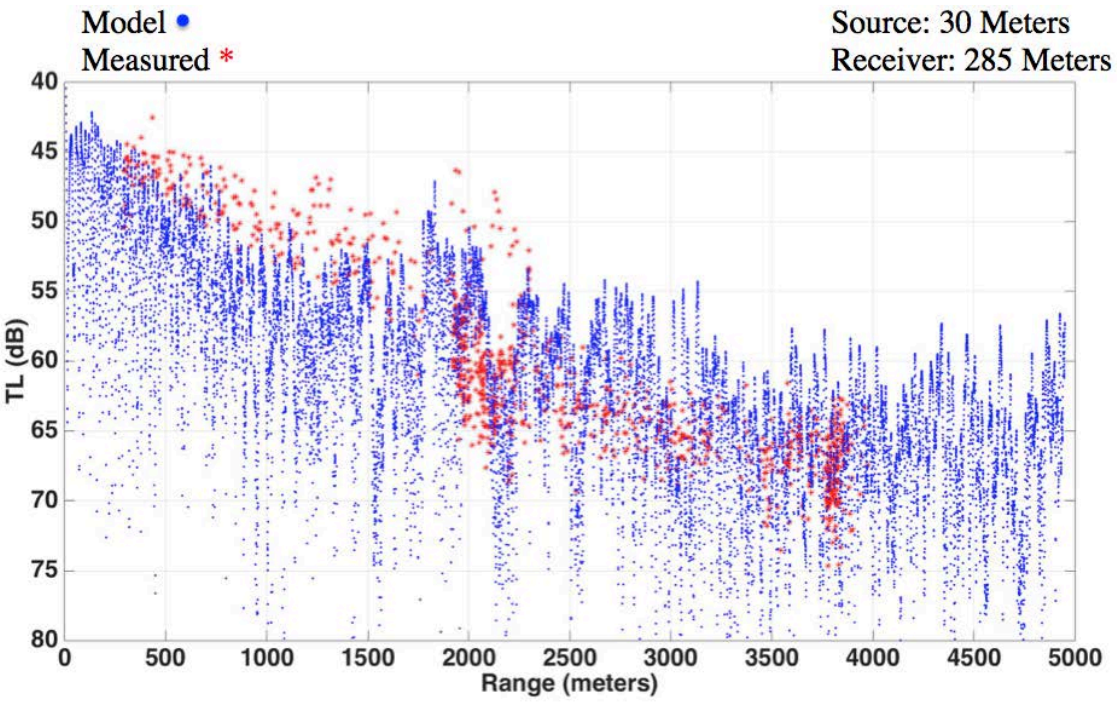

Figure 16. Modeled TL results along the 315° radial (blue dots) and measured TL results (red stars) as a function of horizontal distance from receiver. Source at 30 m depth, receiver at 285 m depth (after Chen and Yeh 2015, personal communication).

As in the measured results, there are two distinct slopes for TL along each radial for the modeled results. Along the 315° radial, there is evidence of some structure around 2000 m which can also be seen in the measured results. It is not an exact comparison between the measured and modeled results because of the lack of bearing dependence for the measured results while the modeled results are for two specific radials.

IV. CONCLUSIONS

Overall, the standard off-the-shelf EMATT performed adequately and demonstrated its utility as a mobile acoustic source for underwater TL measurements. The measured results for TL compared well with the modeled results. There were also lessons learned that could be used in future experiments involving an EMATT as a mobile acoustic source. The EMATT was highly subject to the environmental conditions at the location of the experiment. For the straight-leg track, the EMATT was able to hold course and speed sufficiently but when it began a more complicated geometry, the circular track, it became more difficult to maintain position. Programming the EMATT for basic geometries in the future could help mitigate these effects. The bandwidth for the LFM sweep of the EMATT component in this experiment was constrained as not to interfere with other experiment transmissions occurring over the same time period. Using the full bandwidth allowed by the EMATT in the future would provide a higher SNR. A higher SNR would enable longer range tracking of the EMATT. Deployment of a sonobouy field would also allow for more detailed tracking of the EMATT and for 3-D TL calculations.

In addition to the EMATT deployment explored during this research, there were two additional EMATT deployments during the 2014 SCS Upper-Slope Sand Dunes Experiment. One EMATT followed the same geometry as the EMATT discussed in this research and the second EMATT was programmed to run past the VLA at several different radials to characterize TL as a function of range along different bearings. Future work is recommended using the tools and methodology developed in this work to analyze the remaining data sets. This includes using the remaining recorded data from the Acousonde® receivers and also using the 48 channel VLA that spanned from 37 to 265 m depth to analyze if there was more TL depth dependence.

THIS PAGE INTENTIONALLY LEFT BLANK

LIST OF REFERENCES

Abbot, P., C. Gedney, D. Morton, and C. Emerson, 2006: Mobile Acoustic Source for Underwater Acoustic Measurements. *IEEE Oceans*, Boston, MA, Paper No. 060424-01.

Bendat, J. S., and A. G. Piersol, 1971: *Random Data: Analysis and Measurement Procedures*. Wiley-Interscience, 407 pp.

Clay, C. S., and H. Medwin, 1977: *Acoustical Oceanography*. Wiley-Interscience, 544 pp.

Emery, W. J., and R. E. Thompson, 2004: *Data Analysis Methods in Physical Oceanography*. Elsevier, 638 pp.

Glaser, B. S., 2012: Contingency Planning Memorandum No. 14, Armed Clash in the South China Sea. Council on Foreign Relations, 9 pp. http://i.cfr.org/content/publications/attachments/CPA_contingencymemo_14.pdf

Miller, C. W., C. S. Chiu, D.B. Reeder, Y. J. Yang, L. Chiu, and C. Chen, 2014: Preliminary Observations from the 2014 Sand Dunes Experiment, 79 pp. NPS-OC-14-004.

National Communications System Technology and Standards Division, 1996: Telecommunications: Glossary of Telecommunication Terms. General Services Administration Information Technology Service. [Available online http://www.its.bldrdoc.gov/fs-1037/fs-1037c.htm]

Reeder, D. B., B. B. Ma, and Y. J. Yang, 2010: Very large subaqueous sand dunes on the upper continental slope in the South China Sea generated by episodic, shoaling deep-water internal solitary waves. *Mar. Geol.*, **279**, 12–18, doi: 10.1016/j.margeo.2010.10.009

Reuters, 2015: U.S. Toughens South China Sea Stance. Accessed 13 August 2015. [Available online at http://www.maritime-executive.com/article/us-toughens-south-china-sea-stance.]

Urick, R. J., 1983: *Principles of Underwater Sound.* 3rd ed. Peninsula Publishing, 423 pp.

THIS PAGE INTENTIONALLY LEFT BLANK

INITIAL DISTRIBUTION LIST

1. Defense Technical Information Center
   Ft. Belvoir, Virginia

2. Dudley Knox Library
   Naval Postgraduate School
   Monterey, California